THE JOURNAL OF PHYSICAL CHEMISTRY C

Article

Cite This: J. Phys. Chem. C 2019, 123, 27735−27741

pubs.acs.org/JPCC

Ultrahigh-Pressure Behavior of AO_2 (A = Sn, Pb, Hf) Compounds

Rajkrishna Dutta,*[,†] Boris Kiefer,[‡] Eran Greenberg,[§] Vitali B. Prakapenka,[§] and Thomas S. Duffy[†]

[†]Department of Geosciences, Princeton University, Princeton, New Jersey 08544, United States

[‡]Department of Physics, New Mexico State University, Las Cruces, New Mexico 88011, United States

[§]Center for Advanced Radiation Sources, University of Chicago, Chicago, Illinois 60637, United States

Supporting Information

ABSTRACT: The high-pressure behavior of metal dioxides, AO_2, is of wide interest due to their extensive polymorphism. In this study, high-pressure phase transitions in dioxides of selected group 4 and 14 elements (SnO_2, PbO_2, and HfO_2) were examined by using *in situ* X-ray diffraction in the laser-heated diamond anvil cell to ∼200 GPa and theoretical density functional theory calculations to 600 GPa. The cotunnite-type phase was found to be stable up to the maximum pressure in SnO_2 and PbO_2. For HfO_2, a transition from the cotunnite to the Fe_2P-type phase was observed in experiments at pressures >125 GPa, in agreement with our theoretical computations that predict a transition pressure of 111−137 GPa. Our calculations also predict a re-entrant cotunnite phase in HfO_2 above 305−314 GPa that subsequently transforms into the Ni_2In-type phase at 390−469 GPa. The transition sequences predicted in these oxides are consistent among three different exchange-correlation functionals and can be explained by the energetic competition of stationary electronic flat bands and a pressure-induced shift of electronic states to lower energies.

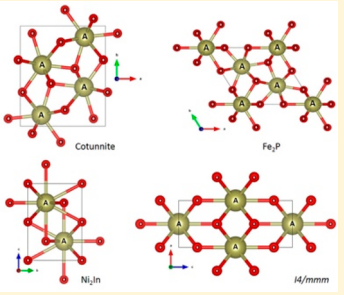

1. INTRODUCTION

There has been long-standing interest in the high-pressure behavior of metal dioxides, AO_2, where A includes group 4 and 14 cations such as Si, Ge, Sn, Pb, Ti, Zr, and Hf.[1] These compounds have been reported to show similar sequences of pressure-induced phase transitions, starting from the rutile-type ($P4_2/mnm$) to the $CaCl_2$- ($Pnnm$), α-PbO_2- ($Pbcn$), and $Pa\bar{3}$-type phase.[2] SiO_2, in particular, has been widely studied because of its geophysical importance. Other group 4 and 14 dioxides have been investigated due to their wide range of technological applications[3−5] and as low-pressure analogues[6] for SiO_2. In general, transition pressures decrease with increasing cation size. Thus, the binary oxides of group 4 and 14 elements provide us an opportunity to study expected ultrahigh-pressure phase transitions relevant to silica at significantly lower pressures.

SiO_2 is the most abundant oxide constituent of the Earth's crust and mantle and is expected to be a major building block of large rocky extrasolar planets. Understanding the mineralogy of rocky extrasolar planets is crucial to constraining their internal structure, thermal behavior, and long-term evolution.[7] Their interior structure will depend on bulk composition, pressure, and temperature. The large size of the super-Earths leads to extremely high internal pressures and temperatures.[8,9] These conditions are often beyond the reach of conventional static high-pressure experimental techniques, and hence our understanding of these bodies is mostly based on theoretical calculations.[10] The use of structural analogues allows experimental study of these phase transitions and benchmarking of theoretical calculations.

In SiO_2, the $Pa\bar{3}$-type (pyrite-type) structure is the highest pressure phase that has been experimentally observed thus far with measurements extending to 268 GPa.[11] Calculations based on density functional theory (DFT) predict a pressure-induced transition from the 6-coordinated (or 6 + 2)[12] $Pa\bar{3}$-type structure to a 9-coordinated cotunnite-type structure (Figure S1, space group $Pnam$) at ∼750 GPa.[13] The cotunnite-type phase has been observed in other metal dioxides and dihalides, but at lower pressures (see Table S1). Based on high-pressure experimental and theoretical studies, several post-cotunnite phases have been proposed. An isosymmetric phase transition from cotunnite-type ($Pnam$) to a 10-coordinated Co_2Si-type ($Pnam$) has been reported in PbF_2,[14,15] UO_2, PuO_2,[16] and several other compounds. The 11-coordinated hexagonal Ni_2In-type ($P6_3/mmc$) structure (observed in SrF_2, CaF_2, and BaF_2)[17] or an orthorhombic distortion ($Pnam$) of it (ThO_2, CeO_2)[18] are other possible post-cotunnite structures. A monoclinic ($P112_1/a$) structure has been observed in the case of $PbCl_2$ and $SnCl_2$.[19] DFT calculations on AO_2 (A = Si, Ge, Ti, Zr) compounds predict a 9-coordinated Fe_2P-type structure ($P\bar{6}2m$) to be energetically favorable with respect to the cotunnite-type structure at high pressure (see Table S1). Laser-heated diamond anvil cell (LHDAC) experiments[20,21] have confirmed the existence of this phase in TiO_2 and ZrO_2 at 210 and 175 GPa, respectively. A recent theoretical investigation using *ab initio* structure searching methods has predicted a 10-fold coordinated

Received: July 18, 2019
Revised: October 4, 2019
Published: October 8, 2019

DOI: 10.1021/acs.jpcc.9b06856
J. Phys. Chem. C 2019, 123, 27735−27741

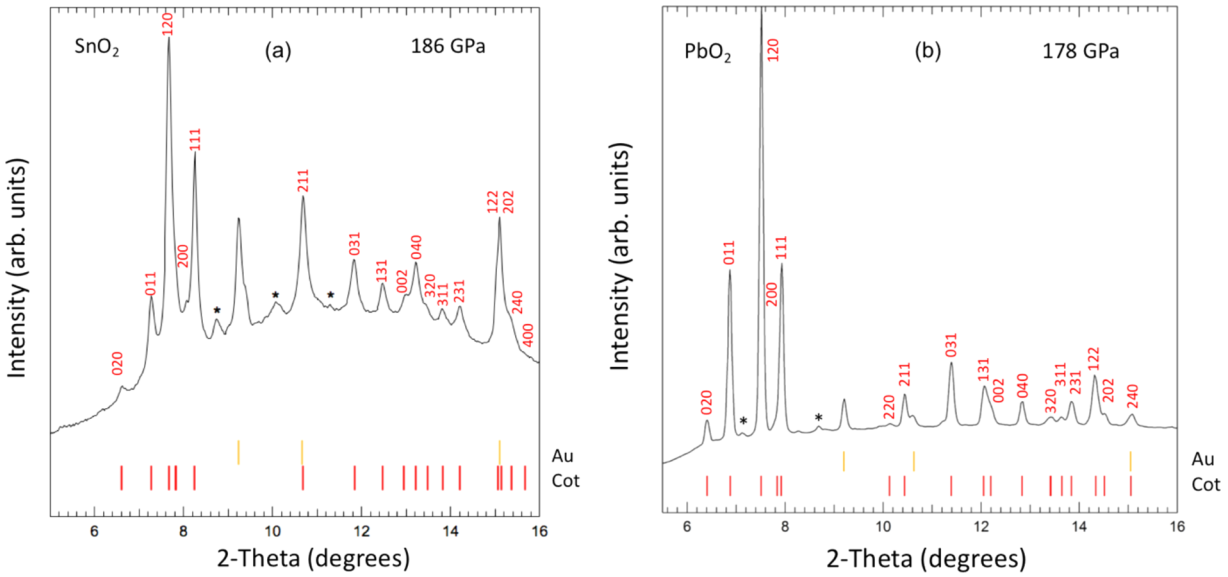

Figure 1. X-ray diffraction patterns of SnO_2 at 186 GPa (a) and PbO_2 at 178 GPa (b). Tick marks at the bottom of each panel indicate the expected peak positions of the cotunnite-type phase (cot, red) and Au (yellow) at these pressures. Asterisks indicate diffraction from untransformed starting material. The Miller indices of the cotunnite-type phase peaks are shown above the measured spectra.

tetragonal structure ($I4/mmm$) to be the stable post-Fe_2P phase in TiO_2 and SiO_2 above 650 and 10000 GPa, respectively.[22] A similar structure has also been proposed in CeO_2 above 450 GPa.[18]

Existing studies[23−26] on selected dioxides of groups 4 and 14, AO_2 (A = Sn, Pb, Hf), are limited to relatively lower pressures, and no conclusive evidence for post-cotunnite phases has been reported. Examination of compounds in these groups enables study of how phase transitions vary with electronic structure and ionic radius. Here, we have performed high pressure and temperature experiments to ∼200 GPa and density functional calculations to 600 GPa to examine cotunnite phase stability and possible post-cotunnite phase transitions. Three different exchange correlation (XC) functionals (GGA: PBE, PBEsol, and meta-GGA: SCAN) were tested to explore the robustness of our results.

2. METHODOLOGY

2.1. Experimental Procedure. Polycrystalline SnO_2 (Alfa Aesar, >99.996% purity), PbO_2 (Alfa Aesar, >99.995% purity), and HfO_2 (Aldrich, >99.95% purity) were examined at ambient conditions by using X-ray diffraction (XRD). In agreement with previous studies,[23−25] they were found to be in the rutile ($P4_2/mnm$), α-PbO_2 ($Pbcn$) + β-PbO_2 ($P4_2/mnm$), and baddeleyite-type ($P2_1/c$) structures. The samples were ground to micrometer-sized grains under acetone and mixed with ∼8 wt % gold. Au served as both the pressure calibrant and laser absorber as described below. Rhenium gaskets were preindented to <20 μm thickness, and ∼20 μm diameter holes were drilled to form the sample chamber. The sample + Au mixtures were then loaded into the sample chamber of symmetric diamond anvil cells with 50 μm culets. The diamond anvils were mounted on tungsten carbide or cubic boron nitride seats for support. No pressure medium was used to maximize the amount of sample at ultrahigh-pressure conditions. Pressure was determined by using the (111) diffraction peak and the equation of state (EOS) of Au.[27,28] Thermal pressures were accounted for by using the Mie-Grüneisen EOS.

In situ angle-dispersive X-ray diffraction was performed at the GSECARS sector (beamline 13-ID-D) of the Advanced Photon Source (APS) using a monochromatic X-ray beam (λ = 0.3344 Å). The X-rays were focused to an ∼3 μm × 3 μm spot size with Kirkpatrick−Baez mirrors. Diffraction patterns were collected by using a Pilatus CdTe 1M detector. Lanthanum hexaboride (LaB_6) was used as a standard to calibrate the position and orientation of the detector. X-ray diffraction patterns were collected for 5−60 s. The two-dimensional X-ray diffraction images were integrated to obtain one-dimensional diffraction patterns by using DIOPTAS.[29] Diffraction peak positions were determined by fitting background subtracted Voigt shapes to the data. Lattice parameters were calculated by using least-squares refinement of the peak positions using UnitCell.[30]

High-pressure phases were synthesized by pulsed heating from both sides by using diode-pumped near-infrared fiber lasers with an ∼15 μm spot size. A pulse generator was used to modulate the power to the two lasers, maximizing the laser power density. The pulses from the lasers were synchronized to each other and to a 1 μs pulse, which served as a gate for the detectors. For each diffraction image, 100000 pulses were typically generated at a rate of 10 kHz (duty cycle of 1%), while for temperature measurement 8−40 frames of 200−10000 accumulations were collected to monitor the stability of the temperature throughout the diffraction measurement. Temperature uncertainties in pulsed laser heating are higher than for continuous heating due to fluctuations between laser pulses. However, the pulsed method has a number of advantages,[31] notably the ability to reach higher temperatures.

2.2. Computational Details. We performed density functional theory (DFT) computations for the cotunnite (OII), Fe_2P, Ni_2In, and $I4/mmm$ phases of SnO_2, PbO_2, and HfO_2. All computations were performed using VASP,[32] a 3D periodic plane wave code. Electrons were treated within the projected augmented wave (PAW) formalism.[33] We considered three different exchange-correlation functionals: PBE,[34] PBEsol,[35] and a recently developed meta-functional, SCAN[36] to cross-validate our results. All computations were performed

DOI: 10.1021/acs.jpcc.9b06856
J. Phys. Chem. C 2019, 123, 27735−27741

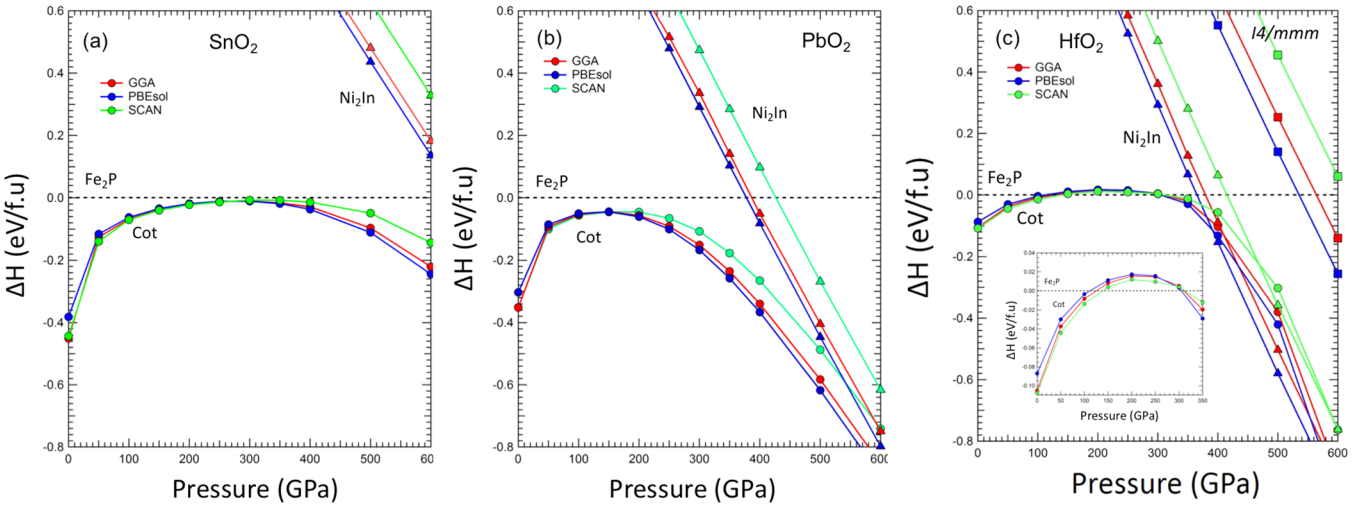

Figure 2. Static enthalpy differences (ΔH) of candidate AO_2 phases with respect to the Fe_2P-type structure (black dashed line) as a function of pressure in (a) SnO_2, (b) PbO_2, and (c) HfO_2. The inset in (c) shows a magnified view of the cotunnite-Fe_2P transition near 200 GPa. The colors represent the different exchange correlation functionals: GGA-PBE (red), PBEsol (blue), and SCAN (green). Symbols indicate the different phases: cotunnite-type (Cot, circles), Ni_2In-type (triangles), and *I*4/*mmm*-type (squares).

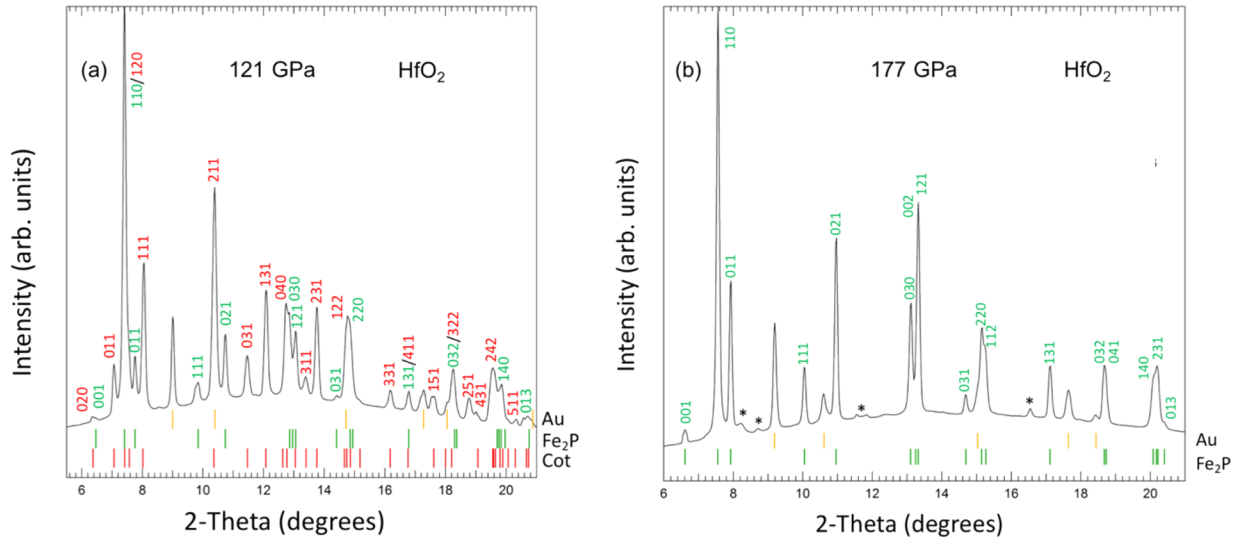

Figure 3. X-ray diffraction pattern of HfO_2 at 121 GPa (a) and 177 GPa (b). The tick marks at the bottom of each panel show the peak positions of Au (yellow), cotunnite-type (red), and Fe_2P-type (green) phases. The Miller indices of the cotunnite- and Fe_2P-type phases are indicated. Asterisks in (b) represent residual cotunnite peaks.

using an energy cutoff, E_{cut} = 700 eV in symmetry preserving mode. Constant density Γ-centered *k*-point grids (*k*-spacing = 0.18) were applied to reduce computational biases in *k*-point sampling due to volume changes and/or different phases. This setting corresponds to a minimum *k*-point sampling of 7 × 12 × 6, 8 × 8 × 12, 13 × 13 × 9, and 14 × 14 × 6 for cotunnite, Fe_2P, Ni_2In, and *I*4/*mmm* phases, respectively. All crystallographically allowed degrees of freedom were optimized simultaneously for pressures up to 600 GPa. Zero-point motion and thermal effects were neglected. The *k*-path for the band structure calculations was chosen following previous work.[37]

3. RESULTS

Experiments were conducted on two group 14 oxides (SnO_2, PbO_2) and one group 4 oxide (HfO_2). For SnO_2, a sample was compressed up to 205 GPa at room temperature followed by pulsed laser heating in steps to a peak temperature of 4090 ± 320 K for a total duration of 30 min. The diffraction pattern obtained on quenching to room temperature (quenched *P* = 186 GPa) could be indexed by using the cotunnite-type structure (Figure 1a). Table S2 compares the observed *d*-spacings for this phase with those obtained from the best fitting unit cell parameters. The maximum difference between the two are <0.002 Å, indicating a good fit to the structure. Static enthalpy differences (ΔH) calculated for different SnO_2 phases with respect to the Fe_2P-type structure are plotted in Figure 2a. The different XC functionals are in very good agreement with each other and show that the cotunnite-type structure is expected to be stable up to at least 600 GPa at 0 K. While the enthalpy difference between the cotunnite- and Fe_2P-type structure decreases with increasing pressure, the Fe_2P-type structure is never energetically favored over the pressure range considered, although the two phases become very close in enthalpy in the 200−400 GPa range.

DOI: 10.1021/acs.jpcc.9b06856
J. Phys. Chem. C 2019, 123, 27735−27741

A second experiment was performed on another group 14 dioxide, PbO_2. In this case, the sample was compressed to 203 GPa and then pulse heated (stepwise) to a maximum temperature of 5360 ± 220 K for 20 min. On quenching to ambient temperature (quenched P = 178 GPa), the X-ray diffraction pattern could be indexed using the cotunnite-type phase (Figure 1b). The small difference (<0.004 Å) between the observed and calculated d-spacings indicates a good fit between our data and the cotunnite-type structure (Table S3). Static enthalpy differences between the Fe_2P- and cotunnite-type structures are larger for PbO_2 than SnO_2 and support our experimental observation. The cotunnite-type phase is energetically favored with respect to both the Fe_2P- and Ni_2In-type structures up to 600 GPa (Figure 2b). A transition to the Ni_2In phase may occur at higher pressures as the enthalpy difference between this phase and cotunnite-type phase shows a decreasing trend with pressure.

We also performed three experimental runs on HfO_2, a group 4 dioxide. In the first run, the sample was cold compressed to 129 GPa and then pulse heated to a peak temperature of 3300 ± 470 K for 20 min and quenched to room temperature (pressure after heating was 121 GPa). The quenched pattern was found to be a mixture of cotunnite- and Fe_2P-type phases (Figure 3a). In the second experiment, a fresh sample was directly compressed up to 206 GPa, heated to 3030 ± 530 K for 10 min, and then quenched (quenched P = 177 GPa). The resulting diffraction pattern indicated that the sample had completely converted to the Fe_2P-type structure (Figure 3b). Tables S4 and S5 compare the observed and calculated d-spacings for representative diffraction patterns. In all cases the residual d-spacings are <0.003 Å, indicating a good fit between the observed and fit peaks. Our *ab initio* calculations are also in excellent agreement with the experimental observations. The Fe_2P-type phase is predicted to become stable with respect to the cotunnite-type phase above 128, 111, and 137 GPa by using PBE, PBEsol, and SCAN functionals, respectively. This is also in good agreement with another recent theoretical study which predicts a transition pressure of ∼120−140 GPa.[26] These authors also suggest that weak peaks observed alongside strong cotunnite-type peaks in their measured diffraction pattern[25] at ∼105 GPa may belong to the Fe_2P-type phase.[26] Our work provides unambiguous evidence for the existence of and complete transformation to this phase.

Our DFT calculations extend to higher pressures than existing computational studies[25,26] and reveal new features of the high-pressure behavior in these systems. We find evidence for a re-entrant cotunnite-type phase (inset Figure 2) above 305−314 GPa in HfO_2, which then undergoes a further pressure-induced transformation into the hexagonal Ni_2In-type structure at 390−469 GPa. The $I4/mmm$ structure was not found to be stable at least up to 600 GPa (Figure 2). This contrasts with the prediction that the Fe_2P-type phase would directly transform to the Ni_2In-type phase at ∼386 GPa.[38] Although the subparallel enthalpy slopes of the Ni_2In and $I4/mmm$ phases (Figure 2) do not allow us to eliminate the possibility of a $P6_3/mmc \rightarrow I4/mmm$ transition at TPa pressures, such a transition is not likely. In general, higher coordination number phases are stabilized with increasing pressure, and the $P6_3/mmc \rightarrow I4/mmm$ transition would require lowering of the coordination number from 11 to 10.

We have also experimentally determined the location and slope of the cotunnite-Fe_2P phase boundary in HfO_2 at high temperatures (Figure 4). In the first run, we heated the sample at 109 GPa and found the cotunnite phase to be stable. On further compression (followed by heating and subsequent quenching), we observed peaks from the Fe_2P-type phase at 144 GPa (3170 ± 660 K), which grew at the expense of the peaks from the cotunnite-type phase with increasing pressure (Figure S2). We have used the first observation of diffraction peaks from a particular structure upon initial heating to identify the stable phase in Figure 4. However, near the phase boundary, peaks from both phases were observed simultaneously. Therefore, in subsequent heating steps, we used a criterion whereby the growth of peaks of one phase and decrease of peaks of the other phase were used to identify the stable phase. In other words, in our compression experiments, the first appearance of peaks from the Fe_2P-type phase has been identified as Fe_2P-type (green circles in Figure 4), and all subsequent higher pressure data points where Fe_2P-type phase peaks increased and cotunnite-type phase peaks decreased in intensity have been labeled as Fe_2P-type. The 2D diffraction patterns showed uniform rings; thus, we believe the observed changes in intensity are a good indicator of phase growth and not texture development.

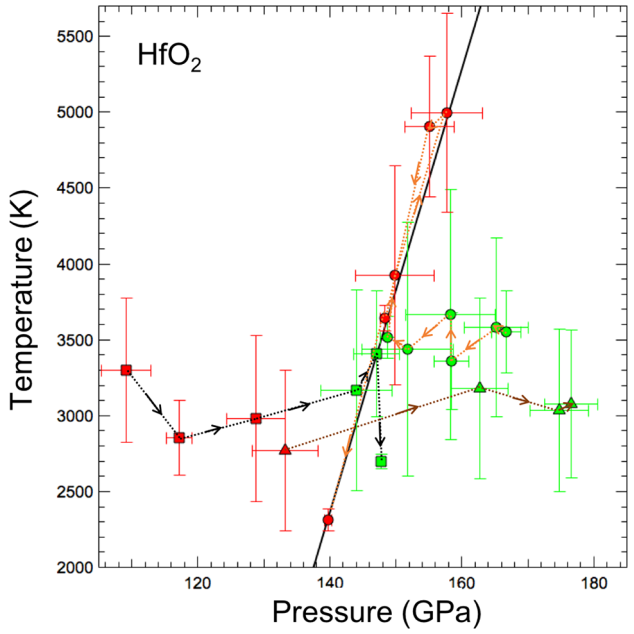

Figure 4. Phase boundary between the cotunnite- and Fe_2P-type phases of HfO_2. Colors (red: cotunnite; green: Fe_2P) represent the different phases. Symbols indicate the different runs, with dashed arrows showing the experimental pathway. The solid black line shows the phase boundary.

In a second run, we directly compressed a HfO_2 sample to 166 GPa and heated it by synthesizing the Fe_2P-type phase. Peaks from the cotunnite-type phase were observed on decompression to 149 GPa (3920 ± 620 K) and increased in intensity with further decrease in pressure followed by heating and then quenching (Figure S2). In the third and final run, a fresh sample was compressed to 133 GPa and heated to 2770 ± 530 K. In this case, strong reflections from the cotunnite-type phase were observed, with minor amounts of the Fe_2P-type phase. On pressurizing to 163 GPa (3180 ± 590 K), the XRD pattern could be indexed by using only the Fe_2P-type phase. These results are all shown in Figure 4, and a phase

DOI: 10.1021/acs.jpcc.9b06856
J. Phys. Chem. C 2019, 123, 27735−27741

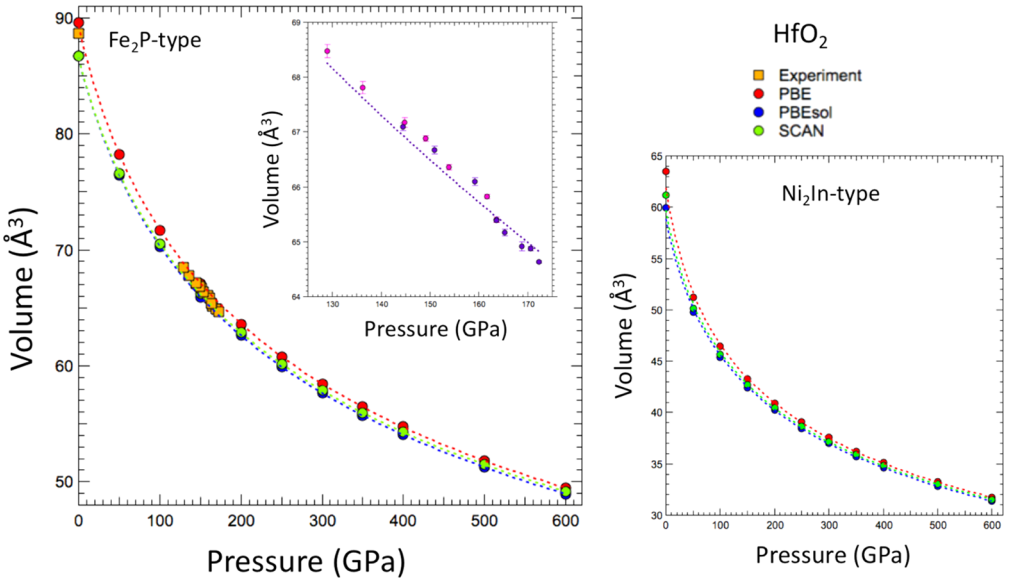

Figure 5. Unit cell volume of Fe_2P- and Ni_2In-type HfO_2 as a function of pressure. Inset shows an expanded view of the experimental data. Dashed lines indicate Birch−Murnaghan EOS fits to the data. In the inset the pink and purple solid symbols have been used to distinguish data obtained during compression and decompression, respectively.

boundary consistent with our observations is indicated. The resulting Clapeyron slope of the phase boundary (+6.9 MPa/K) (Figure 4) is similar to that found in theoretical calculations (+8.0 MPa/K) on the same transition[20] in TiO_2.

Figure S3 shows the unit cell volume of the cotunnite-type phase of all the three oxides as a function of pressure. Our experimental and theoretical calculations are in very good agreement with each other. The relaxed structures for the three XC functionals are also in excellent agreement. Figure 5 shows the unit cell volume of Fe_2P- and Ni_2In-type HfO_2 as a function of pressure. Lattice parameters obtained from experiments and *ab initio* calculations at select pressures are listed in Table S6. At 200 GPa, the GGA-PBE unit cell volumes of SnO_2 (84.1 Å^3) and HfO_2 (84.8 Å^3) in the cotunnite-type phase are comparable while that of PbO_2 (91.4 Å^3) is significantly larger. This is consistent with the ionic radii trends:[39] Pb^{4+} (0.94 Å) > Sn^{4+} (0.81 Å) ≈ Hf^{4+} (0.83 Å). Figure 5 shows the pressure−volume relation of the Fe_2P- and Ni_2In-type phases in HfO_2. In agreement with previous observations in TiO_2[20] and ZrO_2,[21] the cotunnite- to Fe_2P-type transition was found to be accompanied by a small volume change (1.1% at 120 GPa (experiment) and 0.2% at 100 GPa (theory)). In spite of the significant increase in coordination (9 to 11) across the cotunnite- to Ni_2In-type phase transition, it is predicted to have a modest volume collapse of 1.7% at 400 GPa.

The pressure−volume data for HfO_2 (on both compression and decompression) were fitted to the third-order Birch−Murnaghan equation of state:

$$P(V) = \frac{3}{2}K_{0T}\left[\left(\frac{V_0}{V}\right)^{7/3} - \left(\frac{V_0}{V}\right)^{5/3}\right] \times \left\{1 + \frac{3}{4}(K'_{0T} - 4)\left[\left(\frac{V_0}{V}\right)^{2/3} - 1\right]\right\} \quad (1)$$

where P is the pressure, K_T is the isothermal bulk modulus, K'_T is the pressure derivative of the bulk modulus, V is the unit cell volume, and the subscript 0 refers to ambient conditions. The experimental (V_0 = 88.66 Å^3 (fixed), K_{0T} = 283 (1) GPa, and K'_{0T} = 4.2 (fixed)) and theoretical (V_0 = 89.40 Å^3, K_{0T} = 284 GPa, and K'_{0T} = 4.2) equation of state parameters were found to be in excellent agreement. The bulk modulus is also in good agreement with theoretical calculations on TiO_2 (K_{0T} = 287 GPa and K'_{0T} = 4.1)[40] and ZrO_2 (K_{0T} = 272 GPa and K'_{0T} = 4 (fixed)).[21]

4. DISCUSSION AND CONCLUSIONS

Using laser-heated diamond anvil cell experiments and theoretical calculations based on density functional theory, we have studied the high-pressure behavior of three oxides: SnO_2, PbO_2, and HfO_2. The periodic trend predicts that with increasing ionic radii across a group the transition pressure should decrease. The similar transition pressures in hafnia and zirconia (Table S1) are not surprising in view of their comparable ionic radii (Zr^{4+} (0.84 Å) ≈ Hf^{4+} (0.83 Å)). Our study shows that the ultrahigh-pressure behavior of these simple oxides may be more complex than previously realized. Although SnO_2 and PbO_2 form the cotunnite-type phase at relatively low-pressures (74 GPa[23] and 24 GPa,[24] respectively), they were not found undergo any further transitions up to the maximum pressure considered in that work. This agrees with our experiments which show no evidence for the cotunnite → Fe_2P phase transition, at least up to 205 and 203 GPa in SnO_2 and PbO_2 respectively, and DFT computations suggest that this transition is unlikely to occur below 600 GPa. Although, zero-point energy was not considered in our calculations, it is expected to be more positive for the denser (Fe_2P-type) phase, and its vibrational free energy is expected to be less negative. Both effects will tend to stabilize the cotunnite-type phase relative to the Fe_2P-type phase and are thus unlikely to change our results. The Ni_2In-type structure was found to always have substantially higher ΔH and can be ruled out as a possible post-cotunnite phase in SnO_2 or PbO_2. HfO_2, on the other hand, forms the cotunnite-type structure at 14.5 GPa[41] and transforms into the Fe_2P-type structure at 125 GPa. Similar to

DOI: 10.1021/acs.jpcc.9b06856
J. Phys. Chem. C 2019, 123, 27735−27741

ZrO_2,[21] the Fe_2P-type phase in HfO_2 was found to be stable on decompression from 161 GPa to ambient pressure (yielding lattice parameters a = 5.585(2) Å and c = 3.282(1) Å). The Fe_2P-type structure is thus one of the few phases formed at above 1.5 megabar pressures that can be quenched back to ambient conditions without a phase transition or amorphization upon release. The ambient pressure baddeleyite-type ($P2_1/c$) phase[42] of HfO_2 has a volume of 35.1 Å^3/pfu in comparison to 29.5 Å^3/pfu of the quenched Fe_2P-type phase, showing that the quenched phase has a volume decrease of 15.9% compared to the stable ambient structure.

The origin of different phase behavior in these systems can be understood mainly on the basis of their respective electronic structures and their evolution with pressure. In the Fe_2P-type phase, there are extended regions in the Brillouin zone where electronic bands show little dispersion. In contrast to HfO_2, PbO_2 and SnO_2 show two regions with little dispersion: one of them similar to HfO_2 and clearly below the Fermi energy the other flat region defining the highest energy of occupied states (Figure 6a). These low dispersion features do not appear in the corresponding cotunnite-type phases. Therefore, the presence of the larger number of occupied electronic states close to the Fermi level increases the internal energy/enthalpy and thereby stabilizes the cotunnite-type phase relative to the Fe_2P-type phase, and no cotunnite-type → Fe_2P-type phase transition is observed in PbO_2 and SnO_2. In HfO_2, the low-dispersion region is compensated by deeper valleys in the band structure, and the phase transition can occur. With increasing pressure, the flat band in the Fe_2P-type phase does not change much in energy relative to the Fermi energy. In the cotunnite-type phase, no such pinning of electronic states occurs, and its internal energy/enthalpy is lowered by the deepening of the valleys due to a shift of electronic states to lower energies (Figure 6b), stabilizing a re-entrant cotunnite-type phase at 305−314 GPa, prior to its transformation to the Ni_2In-type phase, above 390−469 GPa. Simultaneously, the band gap of the cotunnite-type phase closes, and the character is predicted to change from semiconducting to metallic, characteristic of the Ni_2In-type phase.

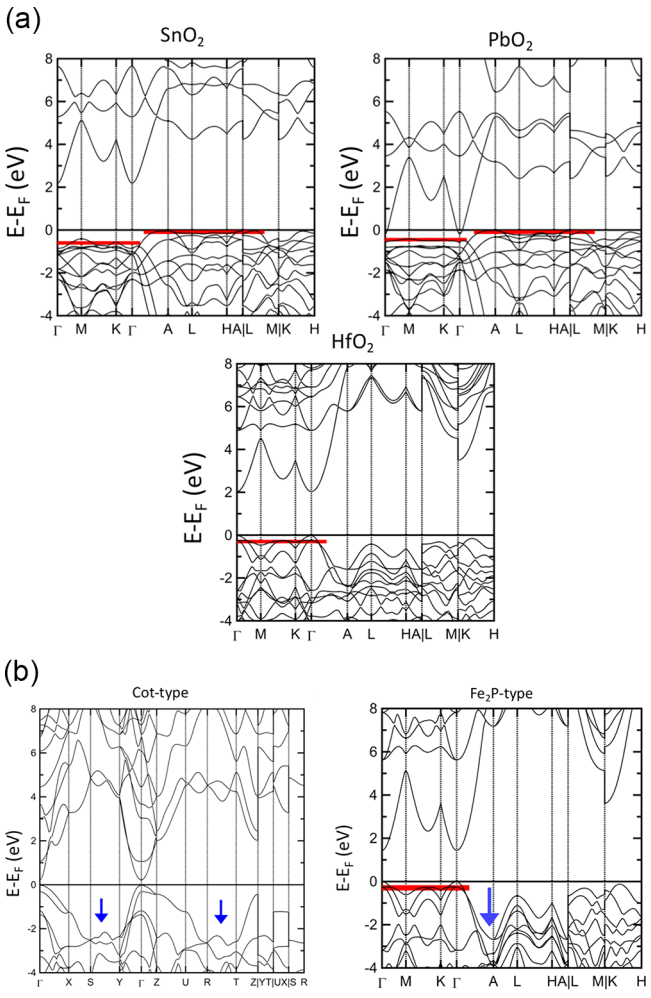

Figure 6. (a) Electronic band structure of the Fe_2P-type phase at 100 GPa. Top left: SnO_2; top right: PbO_2; bottom: HfO_2. E_F is the Fermi energy. The red lines show the flat bands. (b) Electronic band structure of HfO_2 at 500 GPa. Left: cotunnite-type; right: Fe_2P-type. The flat band and the deepening of the valleys are shown with red lines and blue arrows, respectively.

■ ASSOCIATED CONTENT

Supporting Information

The Supporting Information is available free of charge on the ACS Publications website at DOI: 10.1021/acs.jpcc.9b06856.

Comparison of experimental d-spacings from X-ray diffraction with those calculated from best fitting unit cell parameters; representative diffraction patterns used in constraining the cotunnite-type → Fe_2P-type phase boundary in HfO_2; lattice parameters of different AO_2 phases as well as measured and calculated pressure−volume relationships (PDF)

■ AUTHOR INFORMATION

Corresponding Author

*E-mail rd7@princeton.edu.

ORCID

Rajkrishna Dutta: 0000-0001-5651-5626

Notes

The authors declare no competing financial interest.

■ ACKNOWLEDGMENTS

The authors are grateful to S. J. Tracy and S. Tkachev for assistance. This study was funded by the National Science Foundation (NSF, EAR-1415321, and EAR-1836852). Use of the Advanced Photon Source, operated for the U.S. Department of Energy, Office of Science by Argonne National Laboratory, under Contract DE-AC02-06CH11357 is acknowledged. GeoSoilEnviroCARS (GSECARS, Sector 13) is supported by the NSF Earth Sciences (Grant EAR-1634415), and the Department of Energy, Geosciences (Grant DE-FG02-94ER14466), is acknowledged. B.K. acknowledges computing resources provided through the NSF (XSEDE) under Grant DMR TG-110093. The gas-loading facility at GSECARS is partially supported by the Consortium for Materials Properties Research in Earth Sciences under NSF Cooperative Agreement EAR 1606856.

■ REFERENCES

(1) Leger, J. M.; Haines, J. Crystal Chemistry of the AX_2 Compounds under Pressure. *Eur. J. Solid State Inorg. Chem.* **1997**, *37* (7−8), 785−796.

(2) Gracia, L.; Beltrán, A.; Andrés, J. Characterization of the High-Pressure Structures and Phase Transformations in SnO_2. A Density

DOI: 10.1021/acs.jpcc.9b06856
J. Phys. Chem. C 2019, 123, 27735−27741

Functional Theory Study. *J. Phys. Chem. B* **2007**, *111* (23), 6479−6485.
(3) Khoshman, J. M.; Kordesch, M. E. Optical Properties of a-HfO_2 Thin Films. *Surf. Coat. Technol.* **2006**, *201* (6), 3530−3535.
(4) Yu, N.; Gao, L.; Zhao, S.; Wang, Z. Electrodeposited PbO_2 Thin Film as Positive Electrode in PbO_2/AC Hybrid Capacitor. *Electrochim. Acta* **2009**, *54* (14), 3835−3841.
(5) Pusawale, S. N.; Deshmukh, P. R.; Lokhande, C. D. Chemical Synthesis of Nanocrystalline SnO_2 Thin Films for Supercapacitor Application. *Appl. Surf. Sci.* **2011**, *257* (22), 9498−9502.
(6) Umemoto, K.; Wentzcovitch, R. M. Multi-Mbar Phase Transitions in Minerals. *Rev. Mineral. Geochem.* **2010**, *71* (1), 299−314.
(7) Duffy, T.; Madhusudhan, N.; Lee, K. K. M. 2.07 - Mineralogy of Super-Earth Planets. In *Treatise on Geophysics*, 2nd ed.; Schubert, G., Ed.; Elsevier: Oxford, 2015; pp 149−178.
(8) Wagner, F. W.; Tosi, N.; Sohl, F.; Rauer, H.; Spohn, T. Rocky Super-Earth Interiors - Structure and Internal Dynamics of CoRoT-7b and Kepler-10b. *Astron. Astrophys.* **2012**, *541*, A103.
(9) Shahnas, M. H.; Pysklywec, R. N.; Yuen, D. A. Penetrative Convection in Super-Earth Planets: Consequences of $MgSiO_3$ Postperovskite Dissociation Transition and Implications for Super-Earth GJ 876 d. *J. Geophys. Res. E: Planets* **2018**, *123* (8), 2162−2177.
(10) Umemoto, K.; Wentzcovitch, R. M.; Wu, S.; Ji, M.; Wang, C.-Z.; Ho, K.-M. Phase Transitions in $MgSiO_3$ Post-Perovskite in Super-Earth Mantles. *Earth Planet. Sci. Lett.* **2017**, *478*, 40−45.
(11) Kuwayama, Y.; Hirose, K.; Sata, N.; Ohishi, Y. The Pyrite-Type High-Pressure Form of Silica. *Science* **2005**, *309* (5736), 923−925.
(12) Kuwayama, Y.; Hirose, K.; Sata, N.; Ohishi, Y. Pressure-Induced Structural Evolution of Pyrite-Type SiO_2. *Phys. Chem. Miner.* **2011**, *38* (8), 591−597.
(13) Oganov, A. R.; Gillan, M. J.; Price, G. D. Structural Stability of Silica at High Pressures and Temperatures. *Phys. Rev. B: Condens. Matter Mater. Phys.* **2005**, *71* (6), 064104.
(14) Stan, C. V.; Dutta, R.; White, C. E.; Prakapenka, V.; Duffy, T. S. High-Pressure Polymorphism of PbF_2 to 75 GPa. *Phys. Rev. B: Condens. Matter Mater. Phys.* **2016**, *94* (2), 024104.
(15) Haines, J.; Léger, J. M.; Schulte, O. High-Pressure Isosymmetric Phase Transition in Orthorhombic Lead Fluoride. *Phys. Rev. B: Condens. Matter Mater. Phys.* **1998**, *57* (13), 7551−7555.
(16) Song, H. X.; Geng, H. Y.; Wu, Q. Pressure-Induced Group-Subgroup Phase Transitions and Post-Cotunnite Phases in Actinide Dioxides. *Phys. Rev. B: Condens. Matter Mater. Phys.* **2012**, *85* (6), 064110.
(17) Dorfman, S. M.; Jiang, F.; Mao, Z.; Kubo, A.; Meng, Y.; Prakapenka, V. B.; Duffy, T. S. Phase Transitions and Equations of State of Alkaline Earth Fluorides CaF_2, SrF_2, and BaF_2 to Mbar Pressures. *Phys. Rev. B: Condens. Matter Mater. Phys.* **2010**, *81* (17), 174121.
(18) Song, H. X.; Liu, L.; Geng, H. Y.; Wu, Q. First-Principle Study on Structural and Electronic Properties of CeO_2 and ThO_2 under High Pressures. *Phys. Rev. B: Condens. Matter Mater. Phys.* **2013**, *87* (18), 184103.
(19) Léger, J. M.; Haines, J.; Atouf, A. High-Pressure Transitions to a Postcotunnite Phase in Ionic AX_2 Compounds. *Phys. Rev. B: Condens. Matter Mater. Phys.* **1995**, *51* (6), 3902−3905.
(20) Dekura, H.; Tsuchiya, T.; Kuwayama, Y.; Tsuchiya, J. Theoretical and Experimental Evidence for a New Post-Cotunnite Phase of Titanium Dioxide with Significant Optical Absorption. *Phys. Rev. Lett.* **2011**, *107* (4), 045701.
(21) Nishio-Hamane, D.; Dekura, H.; Seto, Y.; Yagi, T. Theoretical and Experimental Evidence for the Post-Cotunnite Phase Transition in Zirconia at High Pressure. *Phys. Chem. Miner.* **2015**, *42* (5), 385−392.
(22) Lyle, M. J.; Pickard, C. J.; Needs, R. J. Prediction of 10-Fold Coordinated TiO_2 and SiO_2 Structures at Multimegabar Pressures. *Proc. Natl. Acad. Sci. U. S. A.* **2015**, *112* (22), 6898−6901.
(23) Shieh, S. R.; Kubo, A.; Duffy, T. S.; Prakapenka, V. B.; Shen, G. High-Pressure Phases in SnO_2 to 117 GPa. *Phys. Rev. B: Condens. Matter Mater. Phys.* **2006**, *73* (1), 014105.
(24) Grocholski, B.; Shim, S.-H.; Cottrell, E.; Prakapenka, V. B. Crystal Structure and Compressibility of Lead Dioxide up to 140 GPa. *Am. Mineral.* **2014**, *99* (1), 170−177.
(25) Al-Khatatbeh, Y.; Lee, K. K. M.; Kiefer, B. Phase Diagram up to 105 GPa and Mechanical Strength of HfO_2. *Phys. Rev. B: Condens. Matter Mater. Phys.* **2010**, *82* (14), 144106.
(26) Al-Khatatbeh, Y.; Tarawneh, K.; Al-Taani, H.; Lee, K. K. M. Theoretical and Experimental Evidence for a Post-Cotunnite Phase Transition in Hafnia at High Pressures. *J. Superhard Mater.* **2018**, *40* (6), 374−383.
(27) Fei, Y.; Ricolleau, A.; Frank, M.; Mibe, K.; Shen, G.; Prakapenka, V. Toward an Internally Consistent Pressure Scale. *Proc. Natl. Acad. Sci. U. S. A.* **2007**, *104* (22), 9182−9186.
(28) Dewaele, A.; Loubeyre, P.; Mezouar, M. Equations of State of Six Metals above 94 GPa. *Phys. Rev. B: Condens. Matter Mater. Phys.* **2004**, *70* (9), 094112.
(29) Prescher, C.; Prakapenka, V. B. DIOPTAS: A Program for Reduction of Two-Dimensional X-Ray Diffraction Data and Data Exploration. *High Pressure Res.* **2015**, *35* (3), 223−230.
(30) Holland, T. J. B.; Redfern, S. A. T. Unit Cell Refinement from Powder Diffraction Data; the Use of Regression Diagnostics. *Mineral. Mag.* **1997**, *61* (1), 65−77.
(31) Goncharov, A. F.; Prakapenka, V. B.; Struzhkin, V. V.; Kantor, I.; Rivers, M. L.; Dalton, D. A. X-Ray Diffraction in the Pulsed Laser Heated Diamond Anvil Cell. *Rev. Sci. Instrum.* **2010**, *81* (11), 113902.
(32) Kresse, G.; Furthmüller, J. Efficient Iterative Schemes for Ab Initio Total-Energy Calculations Using a Plane-Wave Basis Set. *Phys. Rev. B: Condens. Matter Mater. Phys.* **1996**, *54* (16), 11169−11186.
(33) Kresse, G.; Joubert, D. From Ultrasoft Pseudopotentials to the Projector Augmented-Wave Method. *Phys. Rev. B: Condens. Matter Mater. Phys.* **1999**, *59* (3), 1758−1775.
(34) Perdew, J. P.; Burke, K.; Ernzerhof, M. Generalized Gradient Approximation Made Simple. *Phys. Rev. Lett.* **1996**, *77* (18), 3865−3868.
(35) Perdew, J. P.; Ruzsinszky, A.; Csonka, G. I.; Vydrov, O. A.; Scuseria, G. E.; Constantin, L. A.; Zhou, X.; Burke, K. Restoring the Density-Gradient Expansion for Exchange in Solids and Surfaces. *Phys. Rev. Lett.* **2008**, *100* (13), 136406.
(36) Sun, J.; Ruzsinszky, A.; Perdew, J. P. Strongly Constrained and Appropriately Normed Semilocal Density Functional. *Phys. Rev. Lett.* **2015**, *115* (3), 036402.
(37) Setyawan, W.; Curtarolo, S. High-Throughput Electronic Band Structure Calculations: Challenges and Tools. *Comput. Mater. Sci.* **2010**, *49* (2), 299−312.
(38) Al-Khatatbeh, Y.; Tarawneh, K.; Hamad, B. The Prediction of a New High-Pressure Phase of Hafnia Using First-Principles Computations. *IOP Conf. Ser.: Mater. Sci. Eng.* **2018**, *305* (1), 012006.
(39) Shannon, R. D. Revised Effective Ionic Radii and Systematic Studies of Interatomic Distances in Halides and Chalcogenides. *Acta Crystallogr., Sect. A: Cryst. Phys., Diffr., Theor. Gen. Crystallogr.* **1976**, *32* (5), 751−767.
(40) Fu, Z.; Liang, Y.; Wang, S.; Zhong, Z. Structural Phase Transition and Mechanical Properties of TiO_2 under High Pressure. *Phys. Status Solidi B* **2013**, *250* (10), 2206−2214.
(41) Ohtaka, O.; Fukui, H.; Kunisada, T.; Fujisawa, T.; Funakoshi, K.; Utsumi, W.; Irifune, T.; Kuroda, K.; Kikegawa, T. Phase Relations and Volume Changes of Hafnia under High Pressure and High Temperature. *J. Am. Ceram. Soc.* **2001**, *84* (6), 1369−1373.
(42) Adam, J.; Rogers, M. D. The Crystal Structure of ZrO_2 and HfO_2. *Acta Crystallogr.* **1959**, *12* (11), 951−9510000.

DOI: 10.1021/acs.jpcc.9b06856
J. Phys. Chem. C 2019, 123, 27735−27741